Electrochimica Acta 554 (2026) 148339

Contents lists available at ScienceDirect

Electrochimica Acta

journal homepage: www.journals.elsevier.com/electrochimica-acta

Towards robust comparison of distributions of relaxation times

Žiga Gradišar [a,b,*], Žan Gorenc [a,b], Vanja Subotić [c], Pavle Boškoski [a,d]

[a] Jožef Stefan Institute, Jamova cesta 39, 1000 Ljubljana, Slovenia
[b] Jožef Stefan International Postgraduate School, Jamova cesta 39, 1000 Ljubljana, Slovenia
[c] Institute of Thermal Engineering, Graz University of Technology, Inffeldgasse 25/B, 8010 Graz, Austria
[d] Faculty of Information Studies in Novo mesto, jubljanska cesta 30, 8000, Novo mesto, Slovenia

ARTICLE INFO

Dataset link: https://doi.org/10.5281/zenodo.18254178

Keywords:
unbalanced optimal transport
distribution of relaxation times
electrochemical impedance spectroscopy

ABSTRACT

Distribution of relaxation times is a widely used method for the deconvolution of electrochemical impedance spectroscopy data. While proving to be a remarkable lens through which characterisation can be done, it is in practice somewhat impaired by seemingly arbitrary choice for removing ill-posedness of the method. This, together with the rising use of distribution of relaxation times in condition monitoring raises the question of how to fairly compare the distributions. We introduce two complementary methods for comparing distributions of relaxation times: qualitatively via the cumulative distribution of relaxation times and quantitatively using the concept of unbalanced optimal transport. Both approaches relax the importance of regularisation, since they help to discern whether a perceived difference is significant or not. Additionally, the quantitative comparison offers information on the nature of the differences. Specifically, it can distinguish whether the difference can be attributed to a shift in distribution's mass or not. The methodology is applied to experimental electrochemical impedance spectroscopy data from a solid-oxide fuel cell stack.

1. Introduction

Distribution of relaxation times (DRT) together with electrochemical impedance spectroscopy (EIS) is one of most commonly used tools in the analysis of electrochemical systems. DRT uncovers dominant time constants governing the system [1]. The transformation between impedance $Z(j\omega)$ and its corresponding DRT is given by [2]

$$Z(j\omega) := \int_0^\infty \frac{\gamma(\tau)}{1+j\omega\tau}\,\mathrm{d}\tau + R_\infty + j\omega L = \int_{-\infty}^\infty \frac{g(\log\tau)}{1+j\omega\tau}\,\mathrm{d}\log\tau + R_\infty + j\omega L, \tag{1}$$

where R_∞ denotes the high-frequency cut-off resistance and L the inductance. $\gamma(\tau)$ and $g(\log\tau)$ both represent DRT, albeit through different dummy variables — relaxation time and log relaxation time, respectively. Their relation is given by $\tau\gamma(\tau) = g(\log\tau)$. In this work we shall stick with $g(\log\tau)$, since the probed frequencies ω span several orders of magnitude, so $\log\tau$ automatically scales better.

Finding $g(\log\tau)$ defined via the Fredholm integral equation (1) and having only access to noisy measurements of $Z(j\omega)$ is an ill-posed inverse problem [3].

One can always find a larger number of candidates for $g(\log\tau)$ that satisfy (1) than the number of data points.

This is alleviated by imposing constraints like requiring $g(\log\tau)$ to be non-negative and smooth, which is usually done using some form of regularisation like Tikhonov, which can yield adequate approximations of ground truth DRTs [4,5].

Consequently, the results of the analysis can become highly sensitive to the choice of regularisation. This is why a lot of work has gone into methods that help select the appropriate regularisation. It can be chosen using preservation of self-consistency [6], cross-validation [7] or Bayesian approach can be taken [8]. In [9] they used frequency band selection to improve the resolution of regularisation hyperparameter selection. In [10] they modified known regularisation methods for consecutive DRT measurements, while in [11] advanced entropy-based regularisation is applied to obtain a more globally consistent smoothing. There is also a surge in using machine-learning in obtaining DRTs [12,13].

In this paper we tackle the problem how to properly compare DRTs. We introduce a toolkit that helps choosing between different regularisations by indicating if variations in DRT impact impedance deconvolution significantly or not. Within this toolkit condition monitoring is also possible and we show that the importance of precise choice of regularisation subsides in such a context.

Our contribution is two-fold. First, we introduce the qualitative (visual) comparison with cumulative distribution of relaxation times (CDRT). We show that simple transformation makes the visual comparison more proper, since it discards fast variations in the distributions.

* Corresponding author at: Jožef Stefan Institute, Jamova cesta 39, 1000 Ljubljana, Slovenia.
E-mail addresses: ziga.gradisar@ijs.si (Ž. Gradišar), zan.gorenc@ijs.si (Ž. Gorenc), vanja.subotic@tugraz.at (V. Subotić), pavle.boskoski@ijs.si (P. Boškoski).

https://doi.org/10.1016/j.electacta.2026.148339
Received 26 November 2025; Received in revised form 16 January 2026; Accepted 29 January 2026
Available online 30 January 2026

This offers noticeable relaxation in precision needed for choosing an adequate regularisation.

Second, we introduce the quantitative DRTs comparison with unbalanced optimal transport (UOT). This advances the rationale of CDRT, as it provides a user with a scalar, which represents significance of the difference. We also argue that this framework, when carefully constructed, can indicate whether a difference in DRT could be described by processes changing timescale or that new processes have emerged/old processes have died out.

To obtain DRT (*jointly* with R_∞ and L) from noisy EIS measurements we use physics informed autoencoder [14] with implicit regularisation provided by the neural network itself (see [13] for a similar idea) and also with explicit regularisation in form of a customisable degree of smoothness.

2. Visually comparing DRTs: a case for CDRT

Despite being non-negative and a distribution DRT does not in general represent a probability density function (PDF). However, correct normalisation can be achieved trivially by taking the overall polarisation as the normalising constant. In this section we assume that DRT has been normalised accordingly (as done in [2]), so it can be analysed in a probabilistic sense.

With that in mind, we define CDRT, denoted by $G(\log\tau)$, in the same sense as cumulative distribution function (CDF) is defined, i.e., by integrating DRT

$$G(\log\tau) := \int_{-\infty}^{\log\tau} g(\log t)\,\mathrm{d}\log t. \tag{2}$$

We argue that visual comparison of CDRTs is in a sense more fair then visually comparing DRTs. The logic behind is two-fold:

- DRT is already defined via an integral, see (1). Integration inherently smooths out any fast variations. This stems from the fact if $y(t) = \int_{-\infty}^{t} x(\tau)\mathrm{d}\tau$ then $\mathcal{FT}[y](\omega) = \frac{\mathcal{FT}[x](\omega)}{j\omega}$ for $\omega \neq 0$, where $\mathcal{FT}$ denotes Fourier transform. Consequently, any fast variations will have diminishing presence when put through integration. In other words, visually comparing CDRTs can be seen as more fair than comparing DRTs, since fast variations present can present a striking visual difference, while being of little actual importance.
- Another argument comes from probability. There is a concept known as convergence of random variables: if a sequence of random variables $X_1, X_2, \ldots$ with CDFs $F_1, F_2, \ldots$ converges weakly to X with CDF F, that means that $\lim_{n\to\infty} F_n(x) = F(x)$ [15]. We argue that when comparing DRTs, we must at least assume that two equivalent DRTs converge weakly. Hence it is natural that we visually compare their CDFs.[1] In a way, that is also what the famous Kolmogorov–Smirnoff test of equivalence of distributions does — it evaluates the biggest discrepancy between empirical CDFs [16].

The concept of CDRT is showcased in Fig. 1. The top figure shows DRTs obtained from the same EIS data, which was obtained from [17] (for data description see 5.3). One DRT (blue) is estimated with regularisation that penalises fast oscillations, thus resulting in a smooth curve. The other curve (orange) is estimated without such a constraint. Consequently, this results in a curve where multiple sharp spikes are clustered around smooth blue peaks. Bottom plot in Fig. 1 shows the corresponding CDRT curves. Here the visual difference between the blue and orange curves is visually less severe, which we deem beneficial, since they represent the same impedance data. Thus, any large deviations in CDRTs should be taken into account when choosing between solutions, while large deviations in DRTs can mislead with their importance. This is exactly the case in Fig. 1 where orange DRT is hard to visually compare to the blue one, since it has so many peaks. On the other hand, comparing the orange CDRT to the blue one is much easier: they mostly differ around 2 Hz, where the orange DRT identifies local relaxation processes as a bit lower in frequency than the blue CDRT.

As for characterisation of DRTs on their own, it can also be done within this framework, but is comes with caveats. For instance, analysing peaks of DRT changes to analysing steps in CDRT. Specifically, peaks now correspond to the steepest part of the middle of the steps. Consequently, the integrated nature of CDRT *slightly* changes the resolution of positions of the peaks.

Still, CDRT provides only qualitative assessment of differences in relaxation times, while also being well-defined only when compared DRTs are normalised. Such normalisation makes the whole process insensitive to linear scaling as shown in Fig. 2. Both of those limitations, qualitative assessment only and the need for normalisation, can be surpassed using the framework of unbalanced optimal transport.

3. Optimal transport

Before utilising UOT, optimal transport (OT) must be properly introduced. It represents a robust mathematical framework for comparing distributions [18]. The main idea is to define a distance[2] between distributions by how costly is it to transform one distribution to another. Specifically, the distance is defined by how costly is it to transport the probability mass of one distribution to match the other, where transporting costs are defined a priori and the solution is optimal.

Kantorovich's OT distance on a compact metric space X between positive measures $\alpha, \beta \in \mathcal{M}^+(X)$ is given by [19]

$$\mathrm{OT}(\alpha,\beta) := \min_{\pi\in\mathcal{U}(\alpha,\beta)} \int_{X^2} C(x,y)\,\mathrm{d}\pi(x,y), \tag{3}$$

where π is the transport plan, constrained to the set of plans

$$\mathcal{U}(\alpha,\beta) := \left\{\pi \in \mathcal{M}^+(X\times X),\ (p_X)_\sharp\pi = \alpha,\ (p_Y)_\sharp\pi = \beta\right\}. \tag{4}$$

Plans must be such that no transported measure is lost or created anew. In other words, using projections p_X and p_Y we must recover marginal measures (α,β)

$$\begin{aligned}(p_X)_\sharp\pi = \alpha \rightarrow \int_{X^2} f(x)\,\mathrm{d}\pi(x,y) = \int_X f(x)\,\mathrm{d}\alpha(x),\\ (p_Y)_\sharp\pi = \beta \rightarrow \int_{X^2} f(y)\,\mathrm{d}\pi(x,y) = \int_X f(y)\,\mathrm{d}\beta(y),\end{aligned} \tag{5}$$

for any f sufficiently nice. In fact, this ensures $\int_{X^2}\mathrm{d}\pi(x,y) = \int_X \mathrm{d}\beta(x) = \int_X \mathrm{d}\alpha(x)$. $C(x,y)$ is the cost of transportation, usually defined as

$$C(x,y) := d(x,y)^p, \quad p \geq 1, \tag{6}$$

where $d(x,y)$ is a distance, meaning $d(x,y) \geq 0$, $d(x,x) = 0$. $\mathrm{OT}^{1/p}$ is called the p-Wasserstein distance (WD). If sequence of measures α_n is converging to α, then $\mathrm{WD}(\alpha_n,\alpha)$ goes to zero. This means that p-WD metrizes (when the space is compact) the weak convergence [19] — it represents the natural notion of distance in probability space, where probabilities that we consider equivalent converge weakly. This further extends and quantifies our idea of visually comparing DRTs via CDRTs instead (see Section 2), since that idea also leans on the concept of weak convergence.

[1] We could compare their PDFs as well, but that would in general require stronger assumptions.

[2] By "distance" we mean a non-negative scalar of how dissimilar distributions are.

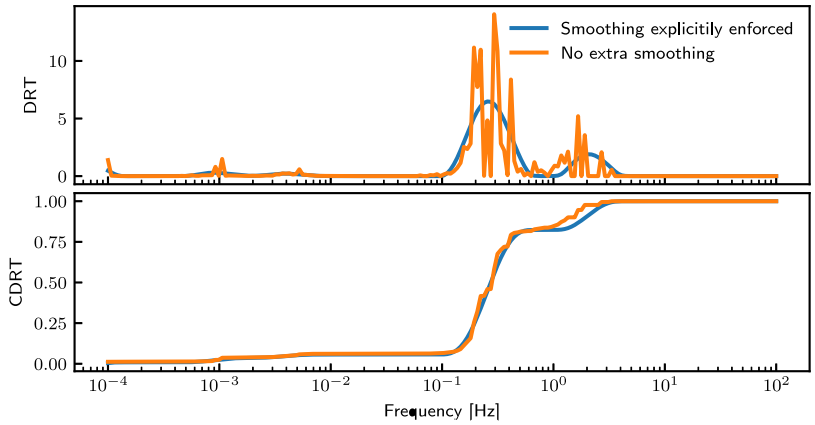

Fig. 1. Estimated DRTs (top) and CDRTs (bottom) with different regularisation settings. We see that assessing significance of differences is easier with CDRT.

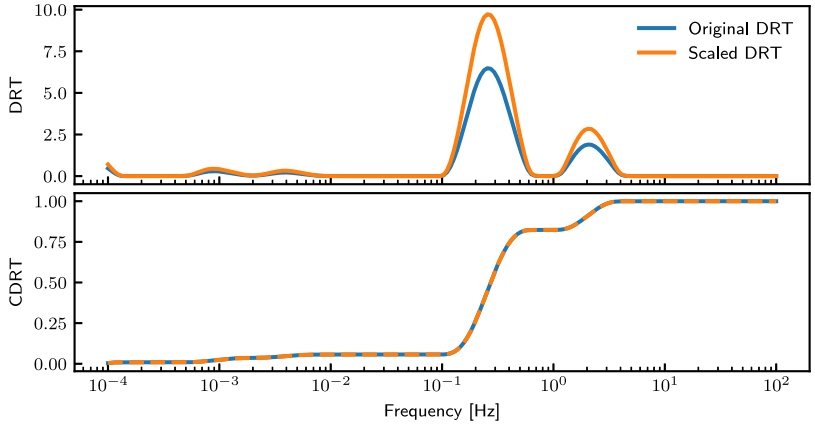

Fig. 2. Comparing DRT and its linearly scaled version (top) is moot if they are normalised like with CDRT (bottom). This showcases an important limitation of CDRT — insensitivity to scaling.

4. Quantitative comparison of DRTs: Unbalanced optimal transport

Here we extend the notion of comparing distributions to comparing positive measures of possibly unequal sizes. UOT between measures $\alpha, \beta \in \mathcal{M}^+(X)$ is given by [19]

$$\mathrm{UOT}(\alpha,\beta) := \inf_{\pi\in\mathcal{M}^+(X^2)} \int_{X^2} C(x,y)\,\mathrm{d}\pi(x,y) + \rho_\alpha \mathrm{D}_\alpha\left((p_X)_\sharp\pi|\alpha\right) + \rho_\beta \mathrm{D}_\beta\left((p_Y)_\sharp\pi|\beta\right) + \epsilon\,\mathrm{KL}\left(\pi|\alpha\otimes\beta\right). \tag{7}$$

π is no longer constrained to $\mathcal{U}(\alpha,\beta)$. Instead, discrepancies between α,β and the marginals $(p_X)_\sharp\pi, (p_Y)_\sharp\pi$ are allowed but punished via penalty terms $\rho_\alpha \mathrm{D}_\alpha\left((p_X)_\sharp\pi|\alpha\right)$ and $\rho_\beta \mathrm{D}_\beta\left((p_Y)_\sharp\pi|\beta\right)$, where D denotes divergence, a notion of difference between measures. ρ_α, ρ_β are constants that allow for balancing of the penalties. Additionally, entropic regularisation term $\epsilon\,\mathrm{KL}(\pi|\alpha\otimes\beta)$ is introduced, where KL is the Kullback–Leibler divergence, given by[3]

$$\mathrm{KL}(\zeta|\eta) := \int_X \log\left(\frac{\mathrm{d}\zeta}{\mathrm{d}\eta}(x)\right)\mathrm{d}\zeta(x) + \int_X \mathrm{d}\eta - \int_X \mathrm{d}\zeta. \tag{8}$$

Note that if α is supported in region where β is not, this divergence grows to $\mathrm{KL}(\alpha|\beta) = +\infty$. Such a regularisation makes the problem strictly convex, making it simpler to solve [19]. Constant ϵ should in general be as small as possible, while permitting calculable and stable solutions.

[3] $\mathrm{d}(\alpha\otimes\beta)(x,y) = \mathrm{d}\alpha(x)\mathrm{d}\beta(y)$.

4.1. Discrete UOT

If measures permit description as

$$\alpha(x) = \sum_{i=1}^{n} \alpha_i \delta(x - x_i), \quad \beta(y) = \sum_{i=1}^{m} \beta_j \delta(y - y_j), \tag{9}$$

as for example empirical measures do, we can restate (7) in a discrete setting

$$\mathrm{UOT}(\boldsymbol{\alpha},\boldsymbol{\beta}) := \min_{\boldsymbol{\Pi}\in\mathbb{R}_+^{n\times m}} \langle \boldsymbol{C},\boldsymbol{\Pi}\rangle + \rho_\alpha \overline{\mathrm{KL}}(\boldsymbol{\pi}_\alpha|\boldsymbol{\alpha}) + \rho_\beta \overline{\mathrm{KL}}(\boldsymbol{\pi}_\beta|\boldsymbol{\beta}) + \epsilon\,\overline{\mathrm{KL}}(\boldsymbol{\Pi}|\boldsymbol{\alpha}\boldsymbol{\beta}^\intercal), \tag{10a}$$

$$\boldsymbol{\pi}_\alpha := \boldsymbol{\Pi}\mathbb{1}_m, \quad \boldsymbol{\pi}_\beta := \boldsymbol{\Pi}^\intercal\mathbb{1}_n, \quad \mathbb{1}_n := [1,1,\dots,1]^\intercal,\ \mathbb{1}_n \in \mathbb{R}^n, \tag{10b}$$

$$\boldsymbol{\alpha} := [\alpha_1,\alpha_2,\dots,\alpha_n]^\intercal, \quad \boldsymbol{\beta} := [\beta_1,\beta_2,\dots,\beta_m]^\intercal, \tag{10c}$$

$$\boldsymbol{C}[i,j] := C(x_i,y_j),\ \boldsymbol{C} \in \mathbb{R}_+^{n\times m}, \tag{10d}$$

$$\langle \boldsymbol{C},\boldsymbol{\Pi}\rangle := \sum_{i=1,j=1}^{n,m} \boldsymbol{C}[i,j]\,\boldsymbol{\Pi}[i,j], \tag{10e}$$

$$\overline{\mathrm{KL}}(\boldsymbol{\zeta}|\boldsymbol{\eta}) := \sum_{i,j} \log\left(\frac{\boldsymbol{\zeta}[i,j]}{\boldsymbol{\eta}[i,j]}\right)\boldsymbol{\zeta}[i,j] + \boldsymbol{\eta}[i,j] - \boldsymbol{\zeta}[i,j], \tag{10f}$$

where instead of general divergences D we have chosen them to be (discrete) Kullback–Leibler, denoted as $\overline{\mathrm{KL}}$. Solving (10a) yields the optimal transport plan $\boldsymbol{\Pi}$, as well as the resulting transported measures from α to β: $\boldsymbol{\pi}_\beta$; and vice versa from β to α: $\boldsymbol{\pi}_\alpha$.

4.2. Solving discrete UOT

We shall be solving (10a) via the Python package [20], which uses the Sinkhorn algorithm as defined in [21], where it was modified to handle UOT problems. Here we mention again that $\epsilon > 0$, otherwise the Sinkhorn algorithm is not expected to converge.

Before solving (10a), one must provide three different parameters: ρ_α, ρ_β and ϵ. As mentioned, ϵ is just a parameter that ensures convergence of the optimisation routine. From another view, the greater it is, the smoother the provided solution $\boldsymbol{\Pi}$ [22, page 18]. We recommend a value that keeps the optimisation stable and yielding results in an acceptable time, and not much greater than that.

The selection of ρ_α to ρ_β is subtle. There are five combinations that can to be considered:

1. $\rho_\alpha, \rho_\beta \to \infty$,
2. $\rho_\alpha, \rho_\beta \to 0$,
3. $\rho_\alpha \gg \rho_\beta$,
4. $\rho_\alpha \ll \rho_\beta$, and
5. $\rho_\alpha \approx \rho_\beta$.

1. Limit $\rho_\alpha, \rho_\beta \to \infty$. For extremely large values of ρ_α and ρ_β UOT reverts back to a balanced case (4) [21], since penalties for a mismatch of $\boldsymbol{\alpha}, \boldsymbol{\beta}$ and $\boldsymbol{\pi}_\alpha, \boldsymbol{\pi}_\beta$, respectively, are too severe to be endured. This forces the transportation plan to preserve all the possible measure, making up/destroying only when absolutely necessary. Such a transport plan is likely to break up peaks of the transported distribution instead of just performing peak matching with the goal distribution.

2. Limit $\rho_\alpha, \rho_\beta \to 0$. If ρ_α, ρ_β go to zero, we can rewrite (10a) to

$$\mathrm{UOT}(\boldsymbol{\alpha}, \boldsymbol{\beta}) := \min_{\boldsymbol{\Pi} \in \mathbb{R}_+^{n \times m}} \langle \boldsymbol{C}, \boldsymbol{\Pi} \rangle + \rho_\alpha \overline{\mathrm{KL}}(\boldsymbol{\pi}_\alpha | \boldsymbol{\alpha}) + \rho_\beta \overline{\mathrm{KL}}(\boldsymbol{\pi}_\beta | \boldsymbol{\beta}) + \epsilon\, \overline{\mathrm{KL}}(\boldsymbol{\Pi} | \boldsymbol{\alpha}\boldsymbol{\beta}^\intercal). \tag{11}$$

Closed form solution for this less restricted problem is given by [22, page 20]

$$\boldsymbol{\Pi}[i,j] = \boldsymbol{\alpha}[i]\, \boldsymbol{\beta}[j]\, e^{-\frac{\boldsymbol{C}[i,j]}{\epsilon}}. \tag{12}$$

Let us assume $\sum_j \boldsymbol{\beta}[j] = 1$. Then

$$\boldsymbol{\pi}_\alpha[i] = \sum_j \boldsymbol{\Pi}[i,j] \to \boldsymbol{\pi}_\alpha[i] \le \boldsymbol{\alpha}[i] \to \sum_i \boldsymbol{\pi}_\alpha[i] \le \sum_i \boldsymbol{\alpha}[i]. \tag{13}$$

It is apparent that we are losing measure in $\boldsymbol{\Pi}$ and exponentially fast for that matter.

Another consequence can be seen if we assume that ϵ is quite small, which means

$$e^{-\frac{\boldsymbol{C}[i,j]}{\epsilon}} \begin{cases} = 1, & \text{if } i = j, \\ \approx 0, & \text{else.} \end{cases} \tag{14}$$

We also assume that $\boldsymbol{\alpha}$ and $\boldsymbol{\beta}$ have peaks at zero and one, respectively

$$\boldsymbol{\alpha}[i] \propto e^{-x_i^2}, \quad \boldsymbol{\beta}[j] \propto e^{-(1-x_j)^2}. \tag{15}$$

Marginals of $\boldsymbol{\Pi}$ are given by

$$\boldsymbol{\pi}_\alpha[i] = \sum_j \boldsymbol{\alpha}[i]\, \boldsymbol{\beta}[j]\, e^{-\frac{\boldsymbol{C}[i,j]}{\epsilon}} \approx \boldsymbol{\alpha}[i]\boldsymbol{\beta}[i], \tag{16}$$

$$\boldsymbol{\pi}_\beta[j] = \sum_j \boldsymbol{\alpha}[i]\, \boldsymbol{\beta}[j]\, e^{-\frac{\boldsymbol{C}[i,j]}{\epsilon}} \approx \boldsymbol{\alpha}[j]\boldsymbol{\beta}[j]. \tag{17}$$

But both $\boldsymbol{\pi}_\alpha$ and $\boldsymbol{\pi}_\beta$ have now peaks around 1/2,[4] meaning a bias has creeped into assessment of $\boldsymbol{\Pi}$.

For both those reasons (transportation losing its job and a bias in the transportation plan) ρ_α, ρ_β should not be too close to zero.

[4] $\mathrm{argmax}_x e^{-x^2} e^{-(1-x)^2} = 1/2$.

3. Case $\rho_\alpha \gg \rho_\beta$. Since $\boldsymbol{\Pi}$ represents transportation plan from $\boldsymbol{\alpha}$ to $\boldsymbol{\beta}$ and vice versa, one can view the discrepancy between $\boldsymbol{\alpha}$ and $\boldsymbol{\pi}_\alpha$ as "work" (local destruction/creation) done on $\boldsymbol{\alpha}$ before sending it to $\boldsymbol{\beta}$. Similarly, one can view difference of $\boldsymbol{\beta}$ to $\boldsymbol{\pi}_\beta$ as "work" being done on $\boldsymbol{\pi}_\beta$ to match $\boldsymbol{\beta}$. If ρ_α is greater than ρ_β then majority of destruction/creation will take place on β side, so from $\boldsymbol{\pi}_\beta$ to $\boldsymbol{\beta}$. This means that creation of new mass is localised (it is created where new processes are suppose to appear in $\boldsymbol{\beta}$), whereas mass that will be destroyed (so old processes that are no more) will be transported before destruction. This makes interpretation of destruction more ambiguous.

4. Case $\rho_\alpha \ll \rho_\beta$. If ρ_α is lower than ρ_β then majority of destruction/creation will take place on α side, so from $\boldsymbol{\alpha}$ to $\boldsymbol{\pi}_\alpha$. This makes destruction of mass localised (old process that have died out are destroyed on the spot), but mass that was created is too be transported (i.e., processes that are new undergo displacement). This makes interpretation of creation more ambiguous.

5. Case $\rho_\alpha \approx \rho_\beta$. This is a mix of the two previous cases. Destruction on α side can be trusted to its location, but it does not show the full picture, since some of the mass that will be destroyed will be transported beforehand. Destruction on β side is all the mass that was cheaper to transport to more favourable positions and then destroyed, so it is not to be trusted when it comes to the location.

Symmetrically, creation on β side can be trusted to its position, but again it does not show the whole picture. Some mass that accounts for new processes can be created on α side and then transported to the correct location.

Assessing absolute values for ρ_α, ρ_β. For simplicity, let us imagine a trivial scenario: we want to optimally transport α to β where both measures are Dirac distributions with $\boldsymbol{\alpha}^\intercal \mathbb{1}_n = \boldsymbol{\beta}^\intercal \mathbb{1}_m = M$. In such a scenario one could expect either the transport to happen in its entirety (no mass creation/destruction) if the measures are close enough, or no transport at all if the measures are far away.

This is not exactly the case when using Kullback–Leibler divergence for penalties for the mismatch of marginals and for the regularisation. To see this, let us solve this scenario on paper. The transport plan $\boldsymbol{\Pi}$ is only going to live on the joint support of α and β. Since both are Dirac measures $\boldsymbol{\Pi}$ is actually a scalar, denoted now by $\hat{\pi}$. In that context, let us solve (10a)

$$\begin{aligned} \mathrm{UOT}(\boldsymbol{\alpha}, \boldsymbol{\beta}) = \min_{\hat{\pi} \ge 0} & c\hat{\pi} + (\rho_\alpha + \rho_\beta)\left(\log\left(\frac{\hat{\pi}}{M}\right)\hat{\pi} + M - \hat{\pi}\right) \\ & + \epsilon\left(\log\left(\frac{\hat{\pi}}{M^2}\right)\hat{\pi} + M^2 - \hat{\pi}\right). \end{aligned} \tag{18}$$

Since the problem is by definition strictly convex and $\hat{\pi}$ is scalar, we can obtain minimum by deriving the upper equation with respect to $\hat{\pi}$

$$0 = c + (\rho_\alpha + \rho_\beta)(\log\hat{\pi} - \log M) + \epsilon\left(\log\hat{\pi} - \log M^2\right). \tag{19}$$

Rearranging the upper term we get

$$\hat{\pi} = M^{\frac{\rho_\alpha + \rho_\beta + 2\epsilon}{\rho_\alpha + \rho_\beta + \epsilon}} \exp\left(-\frac{c}{\rho_\alpha + \rho_\beta + \epsilon}\right). \tag{20}$$

We see that in order to transport a considerable amount of mass, this must hold

$$c < \rho_\alpha + \rho_\beta + \epsilon. \tag{21}$$

Since $c = d(\alpha, \beta)^p$, where $d(\alpha, \beta)$ denotes the distance between measures, we can write

$$d(\alpha, \beta) < \left(\rho_\alpha + \rho_\beta + \epsilon\right)^{1/p}. \tag{22}$$

Now we have a sense of scale for ρ_α and ρ_α. If we want to block significant transportation between two point-distributions above cutoff distance $d(\alpha, \beta)$, we assess ρ_α and ρ_β from (22).

It must also be said that if $c > 0$ mass is being lost immediately, so unless $c \ll \rho_\alpha + \rho_\beta + \epsilon$ one should not expect for the mass to conserve, even if such a solution is seemingly valid.

$$\mathrm{UOT}(\boldsymbol{\alpha},\boldsymbol{\alpha}) = \min_{\boldsymbol{\Pi}\in\mathbb{R}_+^{n\times m}} \langle \boldsymbol{C},\boldsymbol{\Pi}\rangle + \rho_\alpha \overline{\mathrm{KL}}(\boldsymbol{\pi}_\alpha|\boldsymbol{\alpha}) + \rho_\beta \overline{\mathrm{KL}}(\boldsymbol{\pi}_\beta|\boldsymbol{\alpha}) + \epsilon\, \overline{\mathrm{KL}}(\boldsymbol{\Pi}|\boldsymbol{\alpha}\boldsymbol{\alpha}^\intercal) = \tag{23}$$

$$= \epsilon\left(\sum_i \log\left(\frac{\boldsymbol{\alpha}[i]}{\boldsymbol{\alpha}[i]\boldsymbol{\alpha}[i]}\right)\boldsymbol{\alpha}[i] + \boldsymbol{\alpha}[i]\boldsymbol{\alpha}[i] - \boldsymbol{\alpha}[i]\right) = \epsilon\left(\sum_i -\boldsymbol{\alpha}[i]\log(\boldsymbol{\alpha}[i]) + M^2 - M\right) \neq 0$$

Box I.

Which relation between ρ_α and ρ_β to choose. With the sum $\rho_\alpha + \rho_\beta$ constraining the transportation plan, we still need to choose a relation between ρ_α and ρ_β. As explained, any choice can be legitimate, but perhaps the best choice is the one that can be most easily interpreted by the user.

Regularisation bias. As a side effect to introducing regularisation to UOT, the cost of the transport is no longer a distance. Namely, $\mathrm{UOT}(\boldsymbol{\alpha},\boldsymbol{\alpha})$ should be equal to zero, but for $\epsilon \neq 0$ it is not. In case of small ϵ, the optimal transport plan moves nothing, meaning $\boldsymbol{\Pi} = \mathrm{Diag}(\alpha_1, \alpha_2, \dots, \alpha_n)$. Putting this into (10a) gives us the assessment of bias (see Eq. (23) given in Box I), where $\sum_i \boldsymbol{\alpha}[i] = M$. There are ways to redefine UOT to overcome this issue (see [23]), but they are beyond the scope of this paper.

4.3. Simulation

To build intuition we shall be conducting a short study on artificial data, generated by an equivalent circuit model (ECM) of choice. ECM can not only provide familiar looking EIS data, there exists a closed-form transformation from ECM's impedance to DRT. Following Fuoss and Kirkwood [1] we first introduce a change of variable from $j\omega$ to $\log\tau$, i.e. $\hat{Z}(\log\tau) = Z(j\omega)$. The transformation from impedance to DRT is then given by

$$\pi g(\log\tau) = H\left(\log\tau - j\frac{\pi}{2}\right) + H\left(\log\tau + j\frac{\pi}{2}\right), \tag{24}$$

where we have decomposed $\hat{Z}(\log\tau)$ into its real and imaginary part, i.e. $\hat{Z}(\log\tau) = J(\log\tau) - jH(\log\tau)$.

4.3.1. ECM of choice: RQ element

RQ element, also known as Cole–Cole or ZARC, is used to model batteries [24], fuel cells [25] etc. It represents a parallel circuit of a constant phase element and a resistor. In Fuoss–Kirkwood's notation its impedance is given by

$$\hat{Z}_1(\log\tau) := \frac{R_1}{j^{\alpha_1}\exp\left[\alpha_1(\log\tau_1 - \log\tau)\right] + 1}, \tag{25}$$

where R_1 is resistance, α_1 represents deviation from ideal RC circuit and $1/\tau_1$ is the resonance (peak) frequency.

A simple way to naively simulate evolution of DRTs is to translate them. RQ can be translated in location by moving the peak $\tau_1 \to \tau_1 + \Delta\tau_1$. Such a translated impedance is given by

$$\begin{aligned}\hat{Z}_1^{\Delta\tau}(\log\tau) &:= \frac{R_1}{j^{\alpha_1}\exp\left[\alpha_1(\log(\tau_1+\Delta\tau_1) - \log\tau)\right] + 1}\\ &= \frac{R_1}{j^{\alpha_1}\exp\left[\alpha_1(\log\tau_1 - (\log\tau - \log a))\right] + 1}\\ &= \hat{Z}_1(\log\tau - \log a), \quad \text{where } \tau_1 + \Delta\tau_1 = a\tau_1.\end{aligned} \tag{26}$$

This means that change in peak location $\Delta\tau_1$ induces $\hat{Z}$ to shift for $-\log a$. This in turn induces the same shift in DRT

$$\begin{aligned}\pi g_1^{\Delta\tau}(\log\tau) &= H_1\left(\log\tau - \log a - j\frac{\pi}{2}\right) + H_1\left(\log\tau - \log a + j\frac{\pi}{2}\right)\\ &= \pi g_1(\log\tau - \log a).\end{aligned} \tag{27}$$

Another simple imitation of DRT evolution can be made by changing $R_1 \to R_1 + \Delta R_1$, which gives us

$$\begin{aligned}\hat{Z}_1^{\Delta R}(\log\tau) &:= \frac{R_1 + \Delta R_1}{j^{\alpha_1}\exp\left[\alpha_1(\log\tau_1 - \log\tau)\right] + 1}\\ &= \frac{bR_1}{j^{\alpha_1}\exp\left[\alpha_1(\log\tau_1 - \log\tau)\right] + 1}\\ &= b\hat{Z}_1(\log\tau), \quad \text{where } R + \Delta R = bR.\end{aligned} \tag{28}$$

This results in a rescaled DRT

$$\pi g_1^{\Delta R}(\log\tau) = bH_1\left(\log\tau - j\frac{\pi}{2}\right) + bH_1\left(\log\tau + j\frac{\pi}{2}\right) = b\pi g_1(\log\tau). \tag{29}$$

4.3.2. Simulation: fixed parameters of UOT

If one chooses $\rho_\alpha, \rho_\beta, p$, then according to (22) the cutoff transporting distance is $(\rho_\alpha + \rho_\beta + \epsilon)^{1/p}$. Shifting processes at τ for $\Delta\tau$ results in DRTs translating for $-\log(a)$, where $a = \frac{\tau+\Delta\tau}{\tau}$. Cutoff transporting distance then gives us maximal $|\log(a)|$ for the transport to happen. In electrochemistry using logarithm usually means measuring in decades (so using $\log_{10}(\dots)$), but in equations so far we have been using natural logarithm (so $\ln(\dots)$). With that in mind the cutoff transporting distance is given by

$$d_{\mathrm{cut}}^{\log_{10}} = \left|\log_{10}(a)\right| = \frac{|\log(a)|}{\log(10)} = \frac{(\rho_\alpha + \rho_\beta + \epsilon)^{1/p}}{\log(10)}. \tag{30}$$

Choosing $|\log(a)| = \log(\exp[1])$[5] we get

$$\rho_\alpha + \rho_\beta + \epsilon = 1. \tag{31}$$

This in turn gives us

$$d_{\mathrm{cut}}^{\log_{10}} \approx \frac{1}{2.3} \approx 0.43, \tag{32}$$

where $\log(10) \approx 2.3$.

For our toy model we choose a device, represented as a sum of two RQs

- first RQ: $R_1 = 1$, $\tau_1 = 1$, $\alpha_1 = 0.9$,
- second RQ: $R_2 = 1$, $\tau_2 = 1$, $\alpha_2 = 0.9$.

Specifically, we compare the DRTs before and after one of the RQ has shift in peak location, i.e.

$$\boldsymbol{\alpha} = \boldsymbol{g}_1(\log\tau) + \boldsymbol{g}_2(\log\tau), \quad \boldsymbol{\beta} = \boldsymbol{g}_1(\log\tau) + \boldsymbol{g}_2(\log(\tau+\Delta\tau)). \tag{33}$$

There will be four different shifts, one below $d_{\mathrm{cut}}^{\log_{10}}$, one equal and two above:

$$\log_{10}\left(\frac{\tau+\Delta\tau}{\tau}\right) = \left\{\frac{1}{2}\times d_{\mathrm{cut}}^{\log_{10}}, 1\times d_{\mathrm{cut}}^{\log_{10}}, \frac{3}{2}\times d_{\mathrm{cut}}^{\log_{10}}, 2\times d_{\mathrm{cut}}^{\log_{10}}\right\}. \tag{34}$$

The results are shown in Figs. 3 and 4, where we have taken that $\rho_\alpha = \rho_\beta$. Looking at Fig. 3 it is clear that only after the translation of DRT is at or beyond $d_{\mathrm{cut}}^{\log_{10}}$ left peak of $\boldsymbol{\beta}$ is no longer filled up by transportation (great mismatch to the left peak of $\boldsymbol{\pi}_\beta$). This means that UOT's solution argues that a new processes must have been established

[5] For convenience, since $1^{1/p} = 1$.

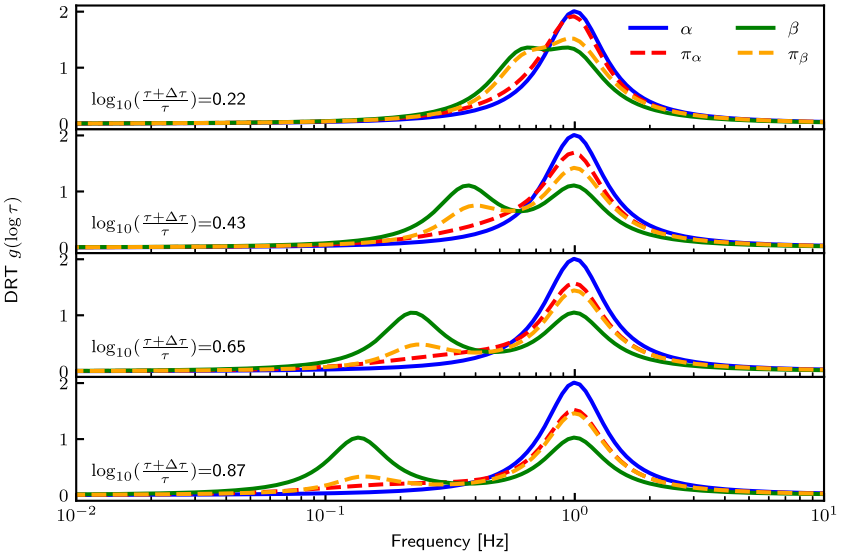

Fig. 3. Solving four different scenarios (four translation cases: less than the transporting cutoff distance, on the cutoff, slightly beyond and far away) of UOT with $\rho_\alpha = \rho_\beta, \epsilon = 0.01, p = 2$. Here we plot $\boldsymbol{\alpha}, \boldsymbol{\pi}_\alpha, \boldsymbol{\beta}, \boldsymbol{\pi}_\beta$. We see that going from top to bottom π_α and π_β start to lose resemblance to α and β, respectively. This indicates that processes are quitting being transported.

here, while mismatch at right peak argues that old process have died out at that location. This is in line with the mismatch of $\boldsymbol{\alpha}$ and $\boldsymbol{\pi}_\alpha$, which suggests the same.

We gain additional information by looking at Fig. 4, the transportation plan $\boldsymbol{\Pi}$. We see that it always tries to at least somewhat compensate the shift, but the further away the shift, the less mass gets moved (the off-diagonal part of the plan get visibly darker). We also see that the plan stays within $\pm d_{\text{cut}}^{\log_{10}}$ of the diagonal, confirming that such a simple benchmark is handy.

4.3.3. Simulation: gauging the parameters of UOT

As mentioned in (22) $(\rho_\alpha + \rho_\beta + \epsilon)^{1/p}$ represents a physically interpretable quantity — cutoff distance for preservation of the relaxation process. If a user is unsure of how to gauge its value, we suggest the following heuristics : compare relaxation processes of the investigated device at two sufficiently distinct set-points. An ideal scenario is simulated in Fig. 5 (top), where two equal RQs translated by Δ are compared. In bottom figure, UOT cost is shown for different $(\rho_\alpha + \rho_\beta + \epsilon)^{1/p}$. The user must decide if

- the relaxation processes endure during the set-point change: green area, where the cost saturates to its maximal value;
- the original relaxation processes are substituted with another processes during the set-point change: red area, where the cost attenuates to the minimal value;
- some relaxation process endure, some do not during the set-point change: yellow area, where the cost changes rapidly due to relaxation processes being either created/destroyed or translated.

Therefore we suggest the user to choose the set-points as such to make the interpretation easier — either when processes just stop to endure (green–yellow boundary as the gauge) or just start to endure (red-yellow boundary as the gauge).

5. Results on experimental data

5.1. Regularisation calibration

As mentioned, UOT can be used calibrate the regularisation of DRTs. In Fig. 6 we compare two (choosing $\rho_\alpha = \rho_\beta = 0.5, \epsilon = 0.001$) DRTs, α and β, from the same EIS measurement, but with different requirements for smoothness of the solution. Data was again taken from [17]. Here we argue that both α and β represent effectively the same DRT.[6] This is because one can transform α to β (and vice versa) without significant mass creation/destruction ($\alpha \approx \pi_\alpha$, $\beta \approx \pi_\beta$), meaning the processes represented at α side are also represented at β side (although they shifted for a bit). On the other hand, if we had sufficient evidence that there are different processes being represented by the two solutions, then an actual decision (using additional knowledge) must be made to choose the better candidate.

5.2. Identification of differences between DRTs

Comparing electrochemical systems before and after some time evolution can be done via comparing DRTs. In exactly that kind of scenario we compare two DRTs, α and β, see Fig. 7. Data was again taken from [17].

There, top figure represents UOT's solution where processes are relatively free to move around, since the cutoff distance is $(\rho_\alpha + \rho_\beta + \epsilon)^{1/2} = \sqrt{2}$. We see from $\alpha \approx \alpha_\pi$ and $\beta \approx \beta\pi$ that all the differences can be attributed to existing processing shifting in their location.

Alternatively, bottom figure represents UOT's solution where processes can only shift for small distances $(\rho_\alpha + \rho_\beta + \epsilon)^{1/2} = \sqrt{0.2}$.

Here the interpretation is much different. For α and β both rightmost peaks do not match π_α and π_β, respectively. This tells us that during transition from α to β some processes have actually died out, which makes this interpretation much different to the first one.

5.3. Condition monitoring in a long-term experiment

Since UOT provides a quantitative approach, we can monitor changes of a device by comparing is current DRT to a reference (nominal) one.

A good set of appropriate data is found in [17], where the authors performed condition monitoring of a 6-cell solid oxide fuel cell stack during a 3600-hour test with short fuel starvation intervals. Eight

[6] Here we assume that the choice for ρ_α and ρ_β makes sense.

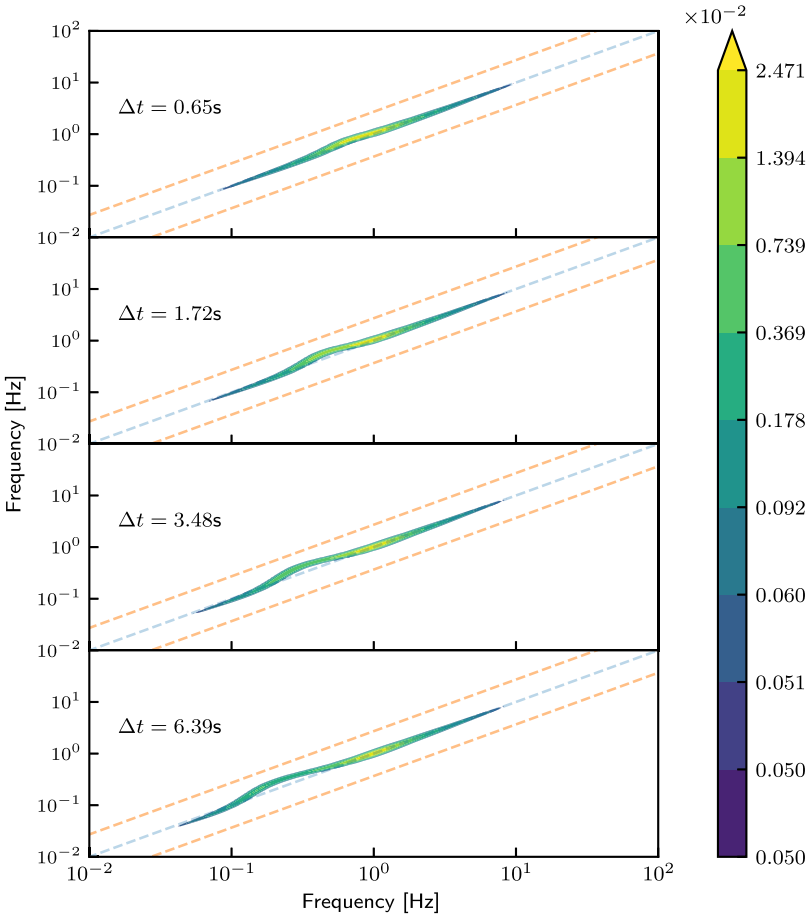

Fig. 4. Solving four different scenarios (four translation cases: less than the transporting cutoff distance, on the cutoff, slightly beyond and far away) of UOT with $\rho_\alpha = \rho_\beta, \epsilon = 0.01, p = 2$. Here we plot $\boldsymbol{\Pi}$ (contour), with added blue dashed line that indicates zero transport distance and two orange dashed lines that indicate a distance of $d_{\text{cut}}^{\log_{10}}$. We see that going from top to bottom $\boldsymbol{\Pi}$ is losing mass that is being transported, which is indicated by the slow discolouration.

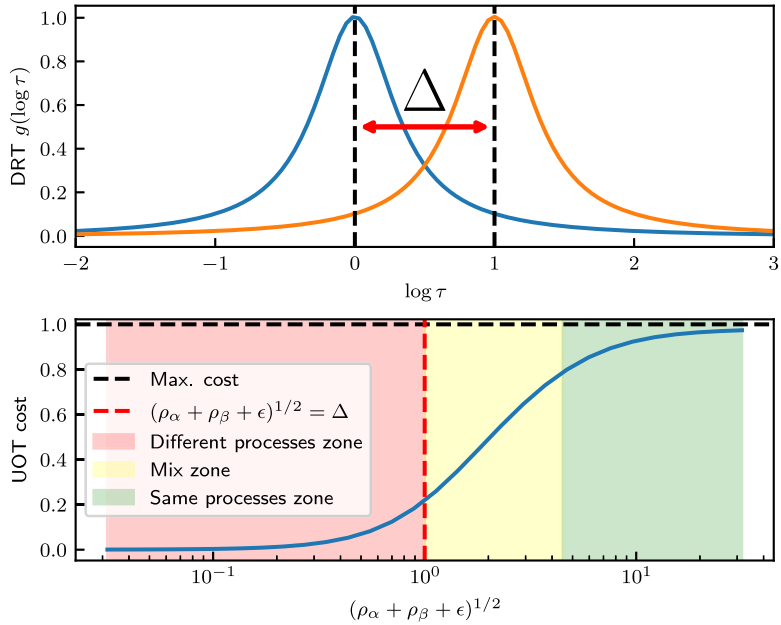

Fig. 5. Gauging the parameters of UOT. (top) Simulation of DRT at different set-points of the investigated device (simple translation of RQ element, where $R = 1, \tau = 1$ and the translation distance is $\Delta = 1$). (bottom) UOT cost in relation to cutoff distance $(\rho_\alpha + \rho_\beta + \epsilon)^{1/2}$, where $\rho_\alpha = \rho_\beta$ and $\epsilon = 0.0001$. Note three different regimes of cost behaviour: where relaxation processes endure (green), where they are created/destroyed (red) and a regime in between (yellow).

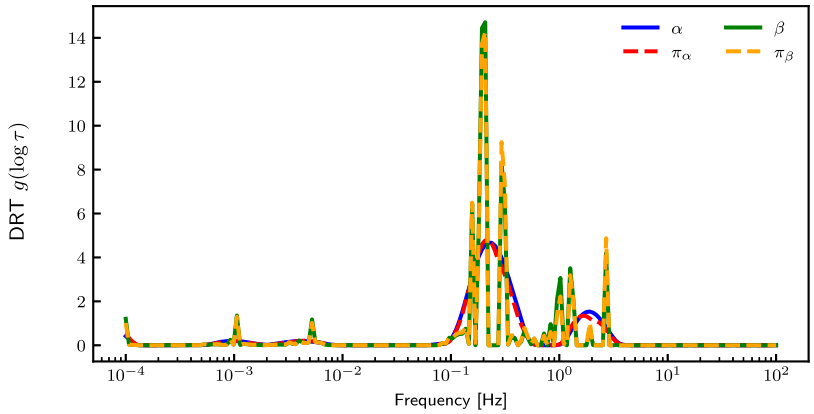

Fig. 6. Utilising UOT ($\rho_\alpha = \rho_\beta = 0.5, \epsilon = 0.001, p = 2$) to compare two DRT candidates, α and β, to represent an EIS measurement. With such parameters the interpretation of the differences is that both DRTs represent the same processes, but they do differ in where those processes are.

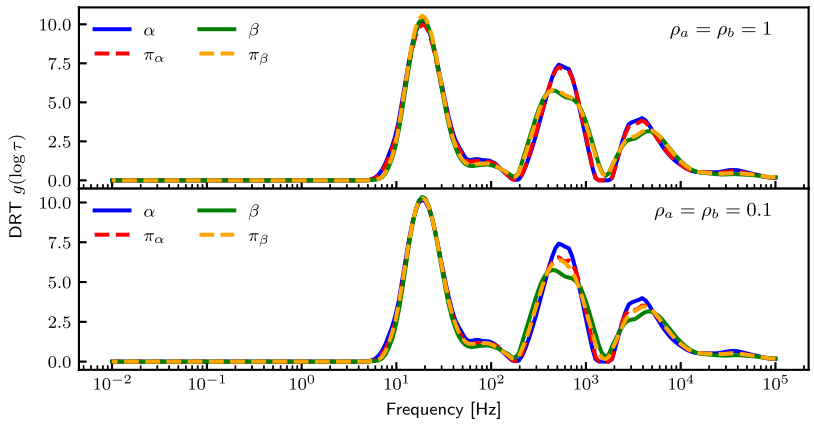

Fig. 7. Comparing DRTs at the beginning and at end of an experiment. Two different choices for ρ_α and ρ_β (both $\epsilon = 0.001, p = 2$) yield two different interpretations of the change: (top) processes have persisted with a slight shift; (bottom) some processes have died out.

different significant events were recognised, which are summed up in Table 1. They obtained more than 600 EIS measurements, which we turned into smooth (extra regularisation) and non-smooth (no extra regularisation) DRTs using [14] (see Fig. 1 for a visual difference between the regularisations).

Fig. 8 shows the results, where we took the 10th EIS measurement as the reference point for comparison. We have chosen $\rho_\alpha = \rho_\beta = 0.5, \epsilon = 0.001$.

Two things are obvious. First, condition monitoring can be performed via UOT, since the obtained metric sharply signals the significant events. Second, the importance of regularisation is meaningfully diminished in this context, since choices for regularisation yield very similar results! This confirms that UOT provides a stable and robust framework for condition monitoring in practical applications.

Table 1
Experiment events in 8 from [17].

Event number	Experiment time [h]	Description
E1	0–40	Start up
E2	270–342	Increased fuel utilisation (decreased fuel flow rate)
E3	582–648	Increased fuel utilisation (increased current)
E4	654–672	Emergency shutdown due to H_2 shortage
E5	1242	Power loss due to thunderstorms
E6	1434	Emergency shutdown due to H_2 shortage
E7	1884–1890	Moving into the new building
E8	2202	Emergency shutdown due to H_2 shortage

6. Conclusion

In field of electrochemistry analysing differences in DRTs is relatively common, yet no deep understanding of what this actually entails was established. Comparing DRTs is a non-trivial problem pertaining to what makes the differences significant and the comparison fair. We provide some much needed insight by introducing two related concepts. For visual comparison we introduce cumulative distribution of relaxation times, which diminishes high-frequency components of DRT, which bear no important information. For qualitative comparison we introduce unbalanced optimal transport, which in addition to giving a scale of how different the distributions are provides transportation and creation/destruction plans. This allows for interpretation in the sense which processes identified by DRT have endured the time evolution versus which have died out/have appeared anew.

Future work. The biggest hurdle to analysis using UOT is the difficulty with interpretation. Namely, arguing that new process have arisen or that the old processes are no more is based entirely on the premise that the interpretation of the UOT's solution is correct. In future work we hope to dispel with those ambiguous decision, perhaps by introducing different discrepancy penalties than Kullback–Leibler that may enable more straight-forward interpretations.

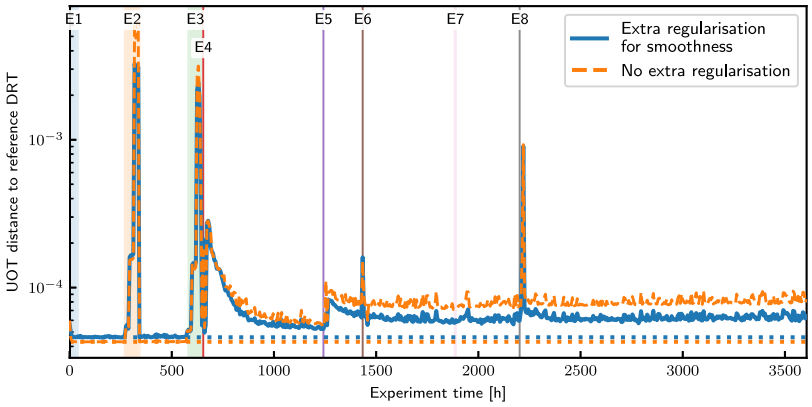

Fig. 8. Evolution of the UOT distance to a reference DRT (10th in order) during the duration of the experiment in [17] together with all events that occurred ($\rho_\alpha = \rho_\beta = 0.5, \epsilon = 0.01, p = 2$). Dotted lines indicate UOT cost bias. Both choices for regularisation yield very similar results.

CRediT authorship contribution statement

Žiga Gradišar: Writing – original draft, Software, Methodology, Investigation, Formal analysis, Conceptualization. **Žan Gorenc:** Software, Conceptualization. **Vanja Subotić:** Supervision, Resources, Investigation, Funding acquisition. **Pavle Boškoski:** Writing – original draft, Resources, Methodology, Investigation, Funding acquisition, Conceptualization.

Funding acknowledgement

The authors express sincere gratitude for the support received for the project "Probabilistic and explainable data-driven modelling of solid-oxide systems" jointly financed by the Slovenian Research and Innovation Agency (ARIS) (project number J2-4452), and the Austrian Science Fund (FWF) (project number I 6251-N). Authors also acknowledge the financial support of the Slovenian Research and Innovation Agency through the research programme P2-0001.

Declaration of competing interest

None.

Data availability

Code together with data is available at https://doi.org/10.5281/zenodo.18254178.

References

[1] R.M. Fuoss, J.G. Kirkwood, Electrical properties of solids. VIII. Dipole moments in polyvinyl chloride-diphenyl systems, J. Am. Chem. Soc. 63 (1941) 385–394, http://dx.doi.org/10.1021/ja01847a013.

[2] C. Plank, T. Rüther, L. Jahn, M. Schamel, J.P. Schmidt, F. Ciucci, M.A. Danzer, A review on the distribution of relaxation times analysis: A powerful tool for process identification of electrochemical systems, J. Power Sources 594 (2024) 233845, http://dx.doi.org/10.1016/j.jpowsour.2023.233845.

[3] T. Paul, P. Chi, P.M. Wu, M. Wu, Computation of distribution of relaxation times by Tikhonov regularization for li ion batteries: usage of l-curve method, Sci. Rep. 11 (2021) 12624.

[4] A.L. Gavrilyuk, D.A. Osinkin, D.I. Bronin, The use of Tikhonov regularization method for calculating the distribution function of relaxation times in impedance spectroscopy, Russ. J. Electrochem. 53 (2017) 575–588, http://dx.doi.org/10.1134/S1023193517060040.

[5] M.E. Orazem, B. Ulgut, The utility and limitations of distribution of relaxation times (drt) methods for impedance analysis, J. Electrochem. Soc. 172 (2025) 073505, http://dx.doi.org/10.1149/1945-7111/adecc8.

[6] M. Saccoccio, T.H. Wan, C. Chen, F. Ciucci, Optimal regularization in distribution of relaxation times applied to electrochemical impedance spectroscopy: ridge and lasso regression methods-a theoretical and experimental study, Electrochim. Acta 147 (2014) 470–482.

[7] A. Maradesa, B. Py, T.H. Wan, M.B. Effat, F. Ciucci, Selecting the regularization parameter in the distribution of relaxation times, J. Electrochem. Soc. 170 (2023) 030502.

[8] M.B. Effat, F. Ciucci, Bayesian and hierarchical Bayesian based regularization for deconvolving the distribution of relaxation times from electrochemical impedance spectroscopy data, Electrochim. Acta 247 (2017) 1117–1129.

[9] P. Carbone, A. De Angelis, A. Bertei, A. Maradesa, F. Ciucci, Optimal regularization for the distribution of relaxation times via frequency-band selection, J. Electrochem. Soc. 172 (2025) 020533, http://dx.doi.org/10.1149/1945-7111/adb5c6.

[10] N. Schlüter, S. Ernst, U. Schröder, Finding the optimal regularization parameter in distribution of relaxation times analysis, ChemElectroChem 6 (2019) 6027–6037, http://dx.doi.org/10.1002/celc.201901863, URL: https://chemistry-europe.onlinelibrary.wiley.com/doi/abs/10.1002/celc.201901863. arXiv:https://chemistry-europe.onlinelibrary.wiley.com/doi/pdf/10.1002/celc.201901863.

[11] B. Py, Z. Wang, Y. Wang, F. Ciucci, Entropy-based regularized regression for advanced distribution of relaxation times deconvolution, J. Power Sources 644 (2025) 236910, http://dx.doi.org/10.1016/j.jpowsour.2025.236910, URL: https://www.sciencedirect.com/science/article/pii/S0378775325007463.

[12] J. Liu, F. Ciucci, The Gaussian process distribution of relaxation times: A machine learning tool for the analysis and prediction of electrochemical impedance spectroscopy data, Electrochim. Acta 331 (2020) 135316.

[13] J. Liu, F. Ciucci, The deep-prior distribution of relaxation times, J. Electrochem. Soc. 167 (2020) 026506.

[14] Žan Gorenc, Žiga Gradišar, P. Boškoski, Learning drts from multiple eis spectra: A neural network approach (working title), 2025, in preparation.

[15] Wikipedia contributors, Convergence of random variables — Wikipedia, the free encyclopedia, 2025, URL: https://en.wikipedia.org/w/index.php?title=Convergence_of_random_variables&oldid=1299281217. [Online; Accessed 7 August 2025].

[16] Wikipedia contributors, Kolmogorov–smirnov test — Wikipedia, the free encyclopedia, 2025, URL: https://en.wikipedia.org/w/index.php?title=Kolmogorov%E2%80%93Smirnov_test&oldid=1289549258. [Online; Accessed 7 August 2025].

[17] G. Nusev, B. Morel, J. Mougin, Đani Juričić, P. Boškoski, Condition monitoring of solid oxide fuel cells by fast electrochemical impedance spectroscopy: A case example of detecting deficiencies in fuel supply, J. Power Sources 489 (2021) 229491, http://dx.doi.org/10.1016/j.jpowsour.2021.229491, URL: https://www.sciencedirect.com/science/article/pii/S0378775321000409.

[18] G. Peyré, M. Cuturi, Computational optimal transport, 2018, http://dx.doi.org/10.48550/ARXIV.1803.00567.

[19] T. Séjourné, G. Peyré, F.-X. Vialard, Unbalanced optimal transport, from theory to numerics, 2023, URL: https://arxiv.org/abs/2211.08775. arXiv:2211.08775.

[20] M. Cuturi, L. Meng-Papaxanthos, Y. Tian, C. Bunne, G. Davis, O. Teboul, Optimal transport tools (ott): A jax toolbox for all things wasserstein, 2022, arXiv preprint arXiv:2201.12324.

[21] C. Frogner, C. Zhang, H. Mobahi, M. Araya-Polo, T. Poggio, Learning with a wasserstein loss, in: Proceedings of the 29th International Conference on Neural Information Processing Systems - Volume 2, NIPS'15, MIT Press, Cambridge, MA, USA, 2015, pp. 2053–2061.

[22] G. Peyré, Course Notes on Computational Optimal Transport, Technical Report, CNRS & DMA, École Normale Supérieure, 2024, URL: https://mathematical-tours.github.io. online lecture notes.

[23] A. Genevay, Sinkhorn divergences: Interpolating between optimal transport and mmd, 2019, Presentation slides, AIP Grenoble. URL: https://audeg.github.io/talks/talkAIP.pdf.

[24] C. Fleischer, W. Waag, H.-M. Heyn, D.U. Sauer, On-line adaptive battery impedance parameter and state estimation considering physical principles in reduced order equivalent circuit battery models: Part 1. Requirements, critical review of methods and modeling, J. Power Sources 260 (2014) 276–291, http://dx.doi.org/10.1016/j.jpowsour.2014.01.129, URL: https://www.sciencedirect.com/science/article/pii/S0378775314002249.

[25] L. Žnidarič, G. Nusev, B. Morel, J. Mougin, Đ. Juričić, P. Boškoski, Evaluating uncertainties in electrochemical impedance spectra of solid oxide fuel cells, Appl. Energy 298 (2021) 117101, http://dx.doi.org/10.1016/j.apenergy.2021.117101, https://www.sciencedirect.com/science/article/pii/S030626192100547X.